Advances in Nano Research, *Vol. 16, No. 5 (2024) 489-500*
https://doi.org/10.12989/anr.2024.16.5.489

Vibration of piezo-magneto-thermoelastic FG nanobeam submerged in fluid with variable nonlocal parameter

Selvamani Rajendran[1], Rubine Loganathan[1], Murat Yaylacı[*2,3,4], Ecren Uzun Yaylacı[5] and Mehmet Emin Özdemir[6]

[1]*Karunya Institute of Technology and Sciences, Coimbatore, Tamilnadu, India*
[2]*Department of Civil Engineering, Recep Tayyip Erdogan University, 53100, Rize, Turkey*
[3]*Turgut Kıran Maritime Faculty, Recep Tayyip Erdogan University, 53900, Rize, Turkey*
[4]*Murat Yaylacı-Luzeri R&D Engineering Company, 53100, Rize, Turkey*
[5]*Faculty of Engineering and Architecture, Recep Tayyip Erdogan University, 53100, Rize, Turkey*
[6]*Department of Civil Engineering, Cankiri Karatekin University, 18100, Çankırı, Turkey*

(*Received February 1 2024, Revised April 11, 2024, Accepted April 15, 2024*)

Abstract. This paper studies the free vibration analysis of the piezo-magneto-thermo-elastic FG nanobeam submerged in a fluid environment. The problem governed by the partial differential equations is determined by refined higher-order State Space Strain Gradient Theory (SSSGT). Hamilton's principle is applied to discretize the differential equation and transform it into a coupled Euler-Lagrange equation. Furthermore, the equations are solved analytically using Navier's solution technique to form stiffness, damping, and mass matrices. Also, the effects of nonlocal ceramic and metal parts over various parameters such as temperature, Magnetic potential and electric voltage on the free vibration are interpreted graphically. A comparison with existing published findings is performed to showcase the precision of the results.
Keywords: FG piezoelectric beam; higher order refined shear deformation theory; spatial nonlocal wave; variable nonlocal elasticity

1. Introduction

A class of Japanese scientists initiated the development of Functionally Graded Materials (FGMs) as a type of composites to regulate the volume fractions of two or more materials in the mixture. The mechanical properties of the developed materials were a matter of curiosity for researchers (Bouazza *et al*. 2019a, b). Due to its layered structure, the effect of flaws occurring in processes such as production on the mechanical behavior of the layers has become one of the essential objectives of contact mechanics. Over the years, many studies examining FGMs under different materials and boundary conditions have been published in the literature (Ellali *et al*. 2018, 2019, 2022, 2024). The continuous and discontinuous contact problems of a functionally graded (FG) layer under the effect of gravity with varying shear modulus and mass density of the beam exponentially were studied by Adiyaman *et al*. (2024). In the study, researchers introduced the buckling behavior of nanobeams using the Euler-Bernoulli beam model, including von Kármán geometrical nonlinearity, which was studied by Alibeigi *et al*. (2018). Arpanahi *et al*. (2023a, b) investigated the buckling behavior of nanoplates at the bottom of a fluid channel. A study by Barretta *et al*. (2018) employed the kinematic model to investigate buckling in beams composed of FG materials exposed to multiple thermal loads. Cuong-Le *et al*. (2022) studied the linear and nonlinear solutions of sigmoid functionally graded material (S-FGM) nanoplates with porous effects. Dehshahri *et al*. (2020) presented the free vibration analysis of nanoplates made of three-directional functionally graded material (TDFGM) with small-scale effects. Ellali *et al*. (2023a, b) examine the wave propagation of an FGM plate through a new model based on high-order displacement theory. They introduce indeterminate integral variables and inverse co-tangential functions to represent shear stress.

Some studies have been carried out that encompass diverse facets. These include studies on the loading of hygro-thermal and bending of electromagnetically responsive piezoelectric nanobeam systems, progressive analysis of intelligent nanostructures, and frequency assessment of functionally graded thin beams after thermal post-buckling Ebrahimi *et al*. (2020). Amara *et al*. (2016) compared the post-buckling behavior of FGM beams with the results obtained from different beam theories using the Hamilton principle and the Navier-type solution method. Using the nth-order shear deformation theory, Becheri *et al*. (2016) presented an exact analytical solution for mechanical buckling analysis of cross-ply laminated plates. Derbale *et al*. (2021) analyzed the thermo-mechanical buckling behavior of composite beams using refined simple and high-order shear deformation theory. Boucheta *et al*. (2024) examined the bending behavior of FGM sandwich surfaces with different core types using the refined hyperbolic plate theory. The vibrational frequency of a two-layered FGM cylindrical shell with and without the effects of internal pressure under ring support is discussed in Ghamkhar *et al*.

*Corresponding author, Ph.D., Professor,
E-mail: murat.yaylaci@erdogan.edu.tr

ISSN: 2287-237X (Print), 2287-2388 (Online)

(2022). The synthesis method of FG-CNTRCs, as well as the static and buckling analysis of FG-CNTRC with piezoelectric layers, was investigated by Heidari *et al.* (2020). Another study by Ke and Wang (2014) explored the Timoshenko beam theory to examine reliable temperature rise, and external electric and magnetic potential, incorporating nonlocal formulations for magneto-electro-elastic vibrations.

The work of Kiani and Eslami (2010) focused on analyzing the propagation of waves in infinite FG plates within a thermal environment. Lafi *et al.* (2024) studied the thermodynamically bending behavior of FG sandwich plates laid on the Winkler/Pasternak/Kerr foundation with various boundary conditions. Li *et al.* (2020) delved into the free vibration analysis of variable thickness beam. Li and Hu (2016) examined the effect of stiffness-softening-hardening of FG beams. Li *et al.* (2009) studied the free vibration of statically thermal post-buckled functionally graded material (FGM) beams with surface-bonded piezoelectric layers subject to both temperature rise and voltage. Graphene sheets were used to model thermo-elastic problems in Lim *et al.* (2015) via Nonlocal Strain Gradient Theory (NSGT). Nguyen *et al.* (2015) proposed a new higher-order shear deformation theory for analyzing buckling and free vibration in isotropic and functionally graded (FG) sandwich beams. Parsa and Mahmoudpour (2019) explored the nonlinear vibration of the conveying fluid submerged in fluid via nonlocal strain gradient elasticity theory. A study by Reddy and El-Borgi (2014) surveyed the variation of natural frequencies using the nonlocal theory on a viscoelastic sheet. Additionally, the distinction of elastic nanobeams driven by stress and strain has been addressed through integral elasticity in Romano and Barretta (2017). Furthermore, researchers investigated the bending of size-dependent magneto-electro-elastic (MEE) nanobeams over nonlinear substrates Shariati *et al.* (2020a). Shariati *et al.* (2020b) investigated the vibration characteristics of flexoelectric nanobeams resting on a viscoelastic foundation and subjected to magneto-electro-viscoelastic-hygro-thermal (MEVHT) loading. The dynamical behavior of an Euler-Bernoulli nanobeam in contact with fluid is discussed by the authors in Sheykhi *et al.* (2023).

In Sun and Luo (2011); Thai and Choi (2012), researchers developed a consistent refined higher-order shear deformation theory (HSDT) to examine the free vibration of functionally graded plates resting on an elastic foundation and to explore the impact of boundary conditions on natural frequencies. In Thai *et al.* (2012), nonlinear bending in nanobeams was discussed using the (FEM) finite element method. Turan *et al.* (2023) discussed an analytical solution based on the first-order shear deformation theory performed for free vibration and buckling analysis of functionally graded porous beams (FGM-P) subjected to various boundary conditions. Vinh and Tounsi (2022a, b) studied the free vibration of functionally graded doubly curved nanoshells and presented findings on the vibration of FG sandwich nanoplates. Vinh *et al.* (2023) investigated the variable nonlocal impact on curved imperfect nanoshells. In addition, exploring research

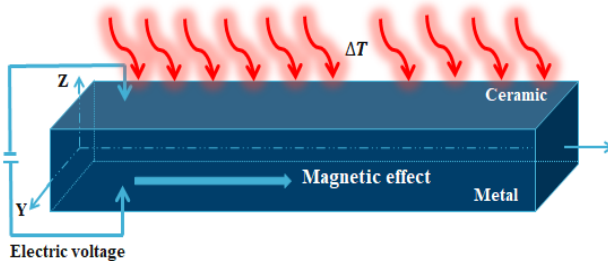

Fig. 1 Geometry of the problem

with varied boundary conditions in the literature can offer readers a more comprehensive perspective on the problem (Kaur *et al.* 2021, 2022, Kaur and Singh 2022, 2023a, b, Yaylacı *et al.* 2022, 2023, 2024). However, vibration analysis of a Functionally Graded (FG) nanobeam submerged in a fluid using modified nonlocal State Space Strain Gradient Theory (SSSGT) has yet to be reported. So, it is crucial to incorporate both variable nonlocal and strain gradient effects in the analysis of submerged FG nanobeam for the first time.

Hence, the behavior of an FG nanobeam submerged in a fluid, in the context of a variable nonlocal parameter, adds accuracy to the model, offering crucial insights into structural deformation that are vital for optimizing performance. Therefore, this study aims to explore the vibration analysis of a Functionally Graded (FG) nanobeam submerged in a fluid using modified nonlocal State Space Strain Gradient Theory (SSSGT). The material properties of the nanobeam, which varies with the magneto piezo thermo elastic effects, are characterized through power law relations, and the equations governing its motion are derived using Hamilton's principle. Later, Navier's solution technique is used to solve for the stiffness, damping, and mass matrices. Additionally, graphical solutions are provided for the dispersion related to fluid viscosity, flow velocity, magnetic effects, and temperature gradient.

2. Problem formulation

An examination of thermo-electro-magneto functionally graded material (FGM) has been carried out using the refined higher-order SSSGT. Fig. 1 depicts the interaction of viscous fluid with its upper surface for an elastic nanobeam positioned at the bottom of a container. Assuming a rigid nature, a solid layer covers the side walls of the fluid container. The nanobeam possesses dimensions including length (L), width (b), and thickness (h). h_f signifies the depth of the fluid atop the beam. In this case, the FGM comprises two distinct sections: a ceramic segment $BaTiO_3$ and a metallic segment $CoFe_2\boldsymbol{O_4}$. q_w represents the force applied externally on the nanobeam along the z-direction. The study incorporates an analysis of the individual components within the FGM to accommodate behaviors influenced by temperature.

In this section, the properties have been computed using power-law relations. The volume fraction of the metallic and ceramic phases is calculated using the power law model

to determine these properties in the thickness direction concerning the temperature variables. Consequently, the fractional volume of the ceramic part can be (Ebrahimi et al. 2021),

$$Vc=zh+12p. \tag{1}$$

While the exponential power law and thickness explore the property distributions in each layer of the nanobeam and the property of material values are considered at local temperature as (Ebrahimi *et al*. 2021),

$$P = P_0(P_{-1}T^{-1} + 1 + P_1T + P_2T^2 + P_3T^3). \tag{2}$$

whereas, $P_0, P_{-1}, P_1, P_2, P_3$ are the coefficients of material phases. The volume fraction of metallic part can be, $V_m = 1 - V_c$.

The fundamental equations for this theory, considering the absence of body related forces, can be expressed in the following manner:

$$\sigma_{ij} = \int_v \alpha(|y'' - y'|, \tau)[C'_{ijkl}\varepsilon_{kl}(y'') - e_{mij}E_m(y'') - \Omega_n(y'') - C'_{ijkl}\alpha_{kl}\Delta T]dV(y'') \tag{3}$$

$$D_i = \int_v \alpha(|y'' - y'|, \tau)[e_{ikl}\varepsilon_{kl}(y'') - E_m(y'') + \Omega_n(y'') - \Delta T]dV(y'') \tag{4}$$

$$B_i = \int_v \alpha(|y'' - y'|, \tau)[\varepsilon_{kl}(y'') + E_m(x') + \chi_{ni}\Omega_n(y'') - \lambda_i\Delta T]dV(y'') \tag{5}$$

Here, the symbols σ_{ij} and ε_{ij} represents stress and strain. E_i and D_i denote the electric field and displacement, while B_i indicates magnetic induction and Ω_i is a magnetic field. The terms α_{kl} and ΔT encompass thermal variation moduli and temperature difference. Furthermore, C'_{ijkl} and e_{mij} represent the elastic and piezoelectric terms. The magnetic constant is denoted as χ_{ij}. Additionally, $\tau = e_0 a/l$ defines the scale coefficient and a, l stands for characteristic lengths within the internal and external facets, $|y'' - y'|$ denotes the Euclidean distance respectively. e_0 is constant of the material considered.

According to the precise kinematic theory that accounts for accurate stress-strain variations in rigid materials, equations of the present problem are designed. Additionally, the higher-order shear deformation theory provides insight into these stress-strain changes. Based on Ebrahimi *et al*. (2021), we consider the refined deformable shear beam's direction as,

$$\prod_x(x, z, \tilde{t}) = \prod(x, \tilde{t}) - \frac{\partial w_b(x, \tilde{t})}{\partial x}z - \frac{\partial w_s(x, \tilde{t})}{\partial x}f^*(z). \tag{6}$$

$$\prod_z(x, z, \tilde{t}) = w_b(x, \tilde{t}) + w_s(x, \tilde{t}). \tag{7}$$

Here, Π, w_b and w_s are the longitudinal, bending and shear components of the transverse displacement. Furthermore, with the intention of shear strain dispersion, $f^*(z)$ is an interpolation function and is taken as (Ebrahimi *et al*. 2021).

$$f^*(z) = \frac{he^z}{h^2 + \pi^2}\left[\pi \sin\left(\frac{\pi z}{h}\right) + h\cos\left(\frac{\pi z}{h}\right)\right] - \frac{h^2}{h^2 + \pi^2}. \tag{8}$$

The nonzero strains can be described using the continuum infinitesimal strain tensor (Ebrahimi *et al*. 2021).

$$\varepsilon_{xx} = \frac{\partial \Pi}{\partial x} - z\frac{\partial^2 w_b}{\partial x^2} - f^*(z)\frac{\partial^2 w_s}{\partial x^2}. \tag{9}$$

$$\gamma_{xz} = g(z)\frac{\partial w_s}{\partial x}. \tag{10}$$

as;

$$g(z) = 1 - \frac{df^*(z)}{dz}. \tag{11}$$

2.1 Modeling the fluid solid interaction

Along the z-direction, the displacement can be differentiated as,

$$v_w = \frac{dw}{d\tilde{t}}. \tag{12}$$

$$\frac{dv_w}{d\tilde{t}} = \frac{d^2w}{d\tilde{t}^2}. \tag{13}$$

Here v_w represents the velocity in the z-direction. Across the z-axis the Navier's Stokes relation (Sheykhi *et al*. 2023) may be stated as follows:

$$\rho f = dvwdt = -\nabla p + \mu f \nabla 2vw. \tag{14}$$

Such as p, μ and ρ_f denotes fluid pressure, viscosity, and density. The above equation can be expanded as Navier's Stokes relation as,

$$\rho_f\frac{dv_w}{d\tilde{t}} = -\frac{\partial p}{\partial z} + \mu_f\left(\frac{\partial^2 v_w}{\partial x^2} + \frac{\partial^2 v_w}{\partial y^2} + \frac{\partial^2 v_w}{\partial z^2}\right). \tag{15}$$

Adhering to the Euler-Bernoulli beam assumptions of Sheykhi *et al*. (2023), the beam allows for the reduction of Eq. (15) as,

$$\rho_f\frac{dv_w}{d\tilde{t}} = -\frac{\partial p}{\partial z} + \mu_f\left(\frac{\partial^2 v_w}{\partial x^2} + \frac{\partial^2 v_w}{\partial y^2}\right). \tag{16}$$

The velocity of the beam in the z-direction is,

$$v_w = \frac{dw}{d\tilde{t}} = \frac{\partial w}{\partial \tilde{t}} + v_x\frac{\partial w}{\partial x} + v_y\frac{\partial w}{\partial y}. \tag{17}$$

While differentiating v_w,

$$\begin{aligned}\frac{dv_w}{d\tilde{t}} &= \frac{\partial}{\partial \tilde{t}}\left(\frac{\partial w}{\partial \tilde{t}} + v_x\frac{\partial w}{\partial x} + v_y\frac{\partial w}{\partial y}\right)\\ &+ v_x\frac{\partial}{\partial x}\left(\frac{\partial w}{\partial \tilde{t}} + v_x\frac{\partial w}{\partial x} + v_y\frac{\partial w}{\partial y}\right)\\ &+ v_y\frac{\partial}{\partial y}\left(\frac{\partial w}{\partial \tilde{t}} + v_x\frac{\partial w}{\partial x} + v_y\frac{\partial w}{\partial y}\right).\end{aligned} \tag{18}$$

Following the use of the simplifications mentioned above in the preceding equations,

$$\frac{dw}{d\tilde{t}} = \frac{\partial w}{\partial \tilde{t}}. \tag{19}$$

$$\frac{dv_w}{d\tilde{t}} = \frac{\partial^2 w}{\partial \tilde{t}^2}. \tag{20}$$

Now, apply the delta operator ~~on~~/to the velocity since$\left(\frac{\partial w}{\partial y} \neq 0\right)$,

$$\nabla 2vw = \nabla 2dwdt = \partial 3w\partial x2\partial t. \tag{21}$$

After the substitution of Eqs. (19-21) into Eq. (16), the pressure gradient exerted by the fluid on the beam surface will be,

$$\frac{\partial p}{\partial z} = -\rho_f \left(\frac{\partial^2 w}{\partial \tilde{t}^2}\right) + \mu_f \left(\frac{\partial^3 w}{\partial x^2 \partial \tilde{t}}\right). \tag{22}$$

In the proposed vibration model, the fluid height (h_f) is multiplied with Eq. (22) to produce the force supplied to the beam from the fluid, and this force is then considered as the external load placed on the beam.

$$\begin{aligned} F_{ext} &= q_w = (A_p)\frac{\partial p}{\partial z} \\ &= -(h_f)\rho_f \left(\frac{\partial^2 w}{\partial \tilde{t}^2}\right) + (h_f)\mu_f \left(\frac{\partial^3 w}{\partial x^2 \partial \tilde{t}}\right). \end{aligned} \tag{23}$$

2.2 Constitutive relations

The constitutive relation of the nanobeam is,

$$\begin{Bmatrix} \sigma_x \\ \tau_{xz} \end{Bmatrix} = \begin{Bmatrix} c_{11} & 0 \\ 0 & c_{66} \end{Bmatrix}. \tag{24}$$

Such as, $c_{11} = \frac{E(z)}{1-\nu^2}; c_{66} = \frac{E(z)}{2(1+\nu)}$.

2.3 Nonlocal elasticity theory

The idea of size-dependent effect, which motivates the mechanical and thermal character of materials, is utilized by a variety of researchers and scientists. To showcase this, classical and non-classical vibration problems are added with the nonlocal theory of elasticity. Adding nonlocal parameters in motion equations amplify the micro-level impact of materials. In the local theory of elasticity, the stress is confined to a single point of the system, whereas in the nonlocal elasticity theory, the elasticity is global and independent of the single point theory Eringen's theory (1983). The notion of nonlocal elasticity theory postulates that the stress experienced at any point is impacted by the strains occurring at all neighbouring points within the continuum body. The nonlocal parameter remains constant and the nonlocal equation with differential term is as follows:

$$(1 - \mu(z)\nabla^2)\sigma_{ij} = S_{ij}.$$

Where $\sigma_{ij}, s_{ij}$are nonlocal stresses and stress tensors, $\nabla^2 = \frac{\partial^2}{\partial x^2} + \frac{\partial^2}{\partial y^2}$is the second Laplace operator, $\mu(z) = (e_0 a)^2$is the nonlocal parameter, $e_0$is a material constant and $a$is an internal characteristic length. This study postulates that the nonlocal parameter undergoes alteration concurrent with the modifications in other material attributes within the functionally graded material.

$$\begin{aligned} \begin{Bmatrix} S_x \\ S_{xz} \end{Bmatrix}^{(n)} &= \begin{Bmatrix} \sigma_x \\ \tau_{xz} \end{Bmatrix}^{(n)} - \mu(z)\nabla^2 \begin{Bmatrix} \sigma_x \\ \tau_{xz} \end{Bmatrix}^{(n)}. \\ &= \begin{bmatrix} c_{11} & 0 \\ 0 & c_{66} \end{bmatrix}^{(n)} \begin{Bmatrix} \varepsilon_x \\ \gamma_{xz} \end{Bmatrix}^{(n)}. \end{aligned} \tag{25}$$

The influence of nonlocal parameters varies along the thickness dimension of functionally graded nanobeam. The connection between nonlocal stress and strain is not solely governed by changes in Poisson's ratio and Young's modulus; it also hinges on variations in the nonlocal parameter.

2.4 Motion Equations

The protracted Lagrangian can be defined via Hamilton's principle as,

$$\tilde{L} = \tilde{\prod} - \tilde{T} + \tilde{V}. \tag{26}$$

Therefore, Hamilton's principle can be expressed as,

$$\delta \int_{\tilde{t}_1}^{\tilde{t}_2} \left(\tilde{\Pi} - \tilde{T} + \tilde{V}\right) d\tilde{t} = 0. \tag{27}$$

In Eq. (27), the variables$\tilde{T}$is the kinetic energy, $\tilde{V}$ is work done and $\tilde{\Pi}$ is strain energy. Hence, the virtual strain energy is,

$$\delta\tilde{\Pi} = \int_V (\sigma_{ij}\delta\varepsilon_{ij} + F_{ext} - D_x E_x - D_z E_z) dv. \tag{28}$$

$$\begin{aligned} &= \int_0^L \int_{\frac{h}{2}}^{\frac{-h}{2}} (\sigma_x \delta\varepsilon_x + \sigma_{xz}\delta\gamma_{xz} - (h_f)\rho_f \left(\frac{\partial^2 w}{\partial \tilde{t}^2}\right) \\ &\quad + (h_f)\mu_f \left(\frac{\partial^3 w}{\partial x^2 \partial \tilde{t}}\right) - D_x \delta E_x - D_z \delta E_z) dz dx \end{aligned} \tag{29}$$

$$\phi(x, z, \tilde{t}) = -\cos(\beta z)\, \phi(x, \tilde{t}) + \frac{2zV_0}{h} e^{-ik\tilde{t}}. \tag{30}$$

where, $D_z = e_{31}\varepsilon_{xx} + e_{33}E_zandD_x = e_{15}\gamma_{xz} + e_{11}E_x$. The electric potential over x axis is$\beta = \pi/h; \phi(x, \tilde{t})$; Ω is the natural frequency of the piezoelectric nanobeam and V_0 is the external electric voltage.

By infusing Eq. (9-10) in Eq. (28),

$$\int_0^L \begin{pmatrix} N\frac{\partial \delta\Pi}{\partial x} - M_b \frac{\partial^2 \delta w_b}{\partial x^2} + (h_f)\rho_f \left(\frac{\partial^2 w}{\partial t^2}\right) \\ -(h_f)\mu_f \left(\frac{\partial^3 w}{\partial x^2 \partial \tilde{t}}\right) - M_s \frac{\partial^2 \delta w_s}{\partial x^2} \\ +Q\frac{\partial \delta w_s}{\partial x} - D_x E_x - D_z E_z \end{pmatrix} dz dx \tag{31}$$

$$= m_0 \frac{\partial^2 w}{\partial \tilde{t}^2} - m_2 \left(\frac{\partial^4 w}{\partial x^2 \partial \tilde{t}^2} + \frac{\partial^4 w}{\partial y^2 \partial \tilde{t}^2} \right)$$

Two constants, $m_0$andm_2, can be acquired from the integrals below, $m_0 = \int_{-\frac{h}{2}}^{\frac{h}{2}} \rho dz$ and $m_2 = \int_{-\frac{h}{2}}^{\frac{h}{2}} \rho z^2 dz$. The stress resultants can be obtained,

$$[N, M_b, M_s] = \int_v [1, z, f(z)] \sigma_{xx} dv. \tag{32}$$

$$Q = \int_v g(z) \sigma_{xz} dv. \tag{33}$$

The kinetic energy of the system can be arrived as,

$$\delta \tilde{T} = \int_v \rho(z) \left[\frac{\partial \Pi_x}{\partial \tilde{t}} \frac{\partial \delta \Pi_x}{\partial \tilde{t}} + \frac{\partial \Pi_z}{\partial \tilde{t}} \frac{\partial \delta \Pi_z}{\partial \tilde{t}} \right] dv. \tag{34}$$

Infusion of Eq. (6-7) in the Eq. (34),

$$\delta \tilde{T} = \int_0^L \begin{pmatrix} I_0^* \left(\frac{\partial \Pi}{\partial \tilde{t}} \frac{\partial \delta \Pi}{\partial \tilde{t}} + \frac{\partial (w_b + w_s)}{\partial \tilde{t}} \frac{\partial \delta (w_b + w_s)}{\partial \tilde{t}} \right) \\ -I_1^* \left(\frac{\partial \Pi}{\partial \tilde{t}} \frac{\partial^2 \delta w_b}{\partial x \partial \tilde{t}} + \frac{\partial^2 w_b}{\partial x \partial \tilde{t}} \frac{\partial \delta \Pi}{\partial \tilde{t}} \right) \\ -J_1^* \left(\frac{\partial \Pi}{\partial \tilde{t}} \frac{\partial^2 \delta w_s}{\partial x \partial \tilde{t}} + \frac{\partial^2 w_s}{\partial x \partial \tilde{t}} \frac{\partial \delta \Pi}{\partial \tilde{t}} \right) \\ +I_2^* \frac{\partial^2 w_b}{\partial x \partial \tilde{t}} \frac{\partial^2 \delta w_b}{\partial x \partial \tilde{t}} + K_2^* \frac{\partial^2 w_s}{\partial x \partial \tilde{t}} \frac{\partial^2 \delta w_s}{\partial x \partial \tilde{t}} \\ +J_2^* \left(\frac{\partial^2 w_b}{\partial x \partial \tilde{t}} \frac{\partial^2 \delta w_s}{\partial x \partial \tilde{t}} + \frac{\partial^2 w_s}{\partial x \partial \tilde{t}} \frac{\partial^2 \delta w_b}{\partial x \partial \tilde{t}} \right) \end{pmatrix} dx. \tag{35}$$

where,

$$f_B = \eta A \Omega_x^2 \frac{\partial^2 w}{\partial x^2}.$$

$$N_T = \int_{-h/2}^{h/2} E(z) \lambda(z) \Delta T dz.$$

whereas, f_B is magnetic force; $\eta$is field permeability; A is cross sectional area of the nanobeam and Ω_x stands for magnetic potential, $N_{x\tilde{t}}$ is the work done along temperature fluctuation due to temperature effect.

$$\delta \tilde{V} = \left(\frac{1}{2} \int_0^l N_{x\tilde{t}} + N_T \left(\frac{\partial w}{\partial x} \frac{\partial \delta w}{\partial x} \right) + \eta \Omega_x^2 \frac{\partial^2 w}{\partial x^2} \right) dx. \tag{36}$$

The beam is treated as having the solid interaction force acting on it as the external load, with the assumption that there is no axial or plane force ($N = 0$),

$$\frac{\partial N}{\partial x} = 0.$$

Deriving the Coupled Euler-Lagrange equation is accomplished by utilizing Eqs. (31, 35-36),

$$\begin{aligned} &\frac{\partial^2 M_b}{\partial x^2} = I_0^* \frac{\partial^2 (w_b + w_s)}{\partial \tilde{t}^2} + I_1^* \frac{\partial^3 \Pi}{\partial x \partial \tilde{t}^2} - I_2^* \frac{\partial^4 w_b}{\partial x^2 \partial \tilde{t}^2} \\ &-J_2^* \frac{\partial^4 w_s}{\partial x^2 \partial \tilde{t}^2} - \left(N_{x\tilde{t}} + N_T \left(\frac{\partial^2 w}{\partial x^2} + \eta \Omega_x^2 \frac{\partial^2 w}{\partial x^2} \right) + q_w \right). \end{aligned} \tag{37}$$

$$\frac{\partial^2 M_s}{\partial x^2} + \frac{\partial Q}{\partial x} - N_x \frac{\partial^2 w}{\partial x^2} = \tag{38}$$

$$\begin{pmatrix} I_0^* \frac{\partial^2 (w_b + w_s)}{\partial \tilde{t}^2} + J_1^* \frac{\partial^3 \Pi}{\partial x \partial \tilde{t}^2} \\ -J_2^* \frac{\partial^4 w_b}{\partial x^2 \partial \tilde{t}^2} - K_2^* \frac{\partial^4 w_s}{\partial x^2 \partial \tilde{t}^2} \end{pmatrix} - \left(N_{x\tilde{t}} + N_T \left(\frac{\partial^2 w}{\partial x^2} + \eta \Omega_x^2 \frac{\partial^2 w}{\partial x^2} \right) \right).$$

$$\delta \phi = \int_{\frac{-h}{2}}^{\frac{h}{2}} \left[cos(\beta z) \left(\frac{\partial Dx}{\partial x} \right) \right] + \beta \, sin(\beta z) \, Dz. \tag{39}$$

where, M^b, M^s and Q^{xz} are the stress resultants and calculated as,

$$\begin{aligned} (M_x^b) &= \sum_{n=1} \int_{h_{n-1}}^{h_n} (S_x)^{(n)} z dz \, . \\ (M_x^s) &= \sum_{n=1} \int_{h_{n-1}}^{h_n} (S_x)^{(n)} f(z) dz \, . \\ (Q_{xz}) &= \sum_{n=1} \int_{h_{n-1}}^{h_n} (S_{xz})^{(n)} g(z) dz \, . \\ (D_{xz}) &= \sum_{n=1} \int_{h_{n-1}}^{h_n} (S_{xz})^{(n)} \phi(z) dz. \end{aligned} \tag{40}$$

where,

$$M^b = \{M_x^b\}, M^s = \{M_x^s\}, Q = \{Q_{xz}\},$$

$$\varepsilon^0 = \{\varepsilon_x^0\}, \varepsilon^1 = \{\varepsilon_x^1\}, \varepsilon^2 = \{\varepsilon_x^2\}, \gamma^0 = \{\gamma_{xz}^0\}.$$

The inertial mass moments can be defined as, $[I_0^*, I_1^*, I_2^*, J_1^*, J_2^*, K_2^*] = \sum_{n=1} \int_{h_{n-1}}^{h_n} \mu(z) \rho(z) \left[1, z, z^2, f^*(z), z f^*(z), f^{2^*}(z)\right] dz$. The material properties considered above are the effective mass density $\rho(z)$ and the effective nonlocal parameter $\mu(z)$. The nonlocal parameter exhibits variations across diverse materials. The variable parameter denoted as $\zeta = \mu_c/\mu_m$ represents the proportion between the ceramic and metal phases. When the nonlocal parameter is constant, ζ equals one ($\zeta = 1$).

3. Analytical solution

In this study, Navier's solution technique is employed to solve the equation of motion.

$$\begin{aligned} \boldsymbol{u}(\boldsymbol{x}, \tilde{\boldsymbol{t}}) &= \sum_{\boldsymbol{n=1}} \boldsymbol{u_n} \, \boldsymbol{cos}\left(\frac{\boldsymbol{n\pi}}{\boldsymbol{l}} \boldsymbol{x}\right) \boldsymbol{e^{i w_n t}}. \\ \boldsymbol{w}(\boldsymbol{x}, \tilde{\boldsymbol{t}}) &= \sum_{\boldsymbol{n=1}} \boldsymbol{w_n} \, \boldsymbol{sin}\left(\frac{\boldsymbol{n\pi}}{\boldsymbol{l}} \boldsymbol{x}\right) \boldsymbol{e^{i w_n t}}. \\ \boldsymbol{Q}(\boldsymbol{x}, \tilde{\boldsymbol{t}}) &= \sum_{\boldsymbol{n=1}} \boldsymbol{Q_n} \, \boldsymbol{cos}\left(\frac{\boldsymbol{n\pi}}{\boldsymbol{l}} \boldsymbol{x}\right) \boldsymbol{e^{i w_n t}}. \\ \boldsymbol{\phi}(\boldsymbol{x}, \tilde{\boldsymbol{t}}) &= \sum_{\boldsymbol{n=1}} \boldsymbol{\phi_n} \, \boldsymbol{sin}\left(\frac{\boldsymbol{n\pi}}{\boldsymbol{l}} \boldsymbol{x}\right) \boldsymbol{e^{i w_n t}}. \\ \begin{Bmatrix} \Pi \\ w_b \\ w_s \end{Bmatrix} &= \begin{Bmatrix} \Pi \, exp[i(\beta x - \Omega \tilde{t})] \\ w_b \, exp[i(\beta x - \Omega \tilde{t})] \\ w_s \, exp[i(\beta x - \Omega \tilde{t})] \end{Bmatrix}. \end{aligned} \tag{41}$$

The amplitudes of the propagating waves are denoted as Π, w_b and w_s whereas Ω and β are the frequency and

wave numbers respectively. By incorporating Eq. (41) into the Eq. (37)-(39), then the attained form will be:

$$\{[K]+[C]\Omega+[M]\Omega^2\}\begin{Bmatrix}\Pi\\ w_b\\ w_s\end{Bmatrix}=0. \tag{42}$$

From the above definition, $[K]$ represents stiffness, $[C]$ stands for damping, and $[M]$ is for mass matrices. The elements of these matrices are:

$$k_{11}=(1+\lambda^2\beta^2)A_{xx}\beta^2.$$

$$k_{12}=i(N_{x\tilde{t}}+\eta\Omega_x^2+q_w)(1+\lambda^2\beta^2)B_{xx}\beta^5.$$

$$k_{13}=i(N_{x\tilde{t}}+\eta\Omega_x^2+q_w)(1+\lambda^2\beta^2)B^s_{xx}\beta^5.$$

$$k_{14}=e_{31}(1-\lambda^2\beta^2)\beta\, sin(\beta z)\phi-\frac{2V_0e^{ik\tilde{t}}}{h}.$$

$$k_{22}=-(N_{x\tilde{t}}+\eta\Omega_x^2+q_w)N_T(1+\lambda^2\beta^2)D_{xx}\beta^6. \tag{43}$$

$$k_{23}=-(N_{x\tilde{t}}+\eta\Omega_x^2+q_w)N_T(1+\lambda^2\beta^2)D^s_{xx}\beta^6.$$

$$k_{24}=e_{31}(1-\lambda^2\beta^2)\beta\, sin(\beta z)\phi-\frac{2V_0e^{ik\tilde{t}}}{h}.$$

$$k_{33}=-(N_{x\tilde{t}}+\eta\Omega_x^2+q_w)N_T(1+\lambda^2\beta^2)(H^s_{xx}\beta^6+A^s\beta^4).$$

$$k_{34}=e_{31}(1-\lambda^2\beta^2)\beta^2\, sin(\beta z)\phi-\frac{2V_0e^{ik\tilde{t}}}{h}.$$

$$c_{11}=-A_{xx}\tau\beta^2.$$

$$c_{12}=i(N_{x\tilde{t}}+\eta\Omega_x^2)B_{xx}\tau\beta^5.$$

$$c_{13}=i(N_{x\tilde{t}}+\eta\Omega_x^2)B^s_{xx}\tau\beta^5.$$

$$c_{14}=\tau e_{31}\left(\beta^2\, cos(\beta z)\frac{dz}{dt}\phi-\left(\frac{2V_0e^{ik\tilde{t}}}{h}(ik)\right)\right).$$

$$c_{22}=-(N_{x\tilde{t}}+\eta\Omega_x^2)D_{xx}\tau\beta^6. \tag{44}$$

$$c_{23}=-(N_{x\tilde{t}}+\eta\Omega_x^2)D^s_{xx}\tau\beta^6.$$

$$c_{24}=\tau e_{31}\left(\beta^2\, cos(\beta z)\frac{dz}{dt}\phi-\left(\frac{2V_0e^{ik\tilde{t}}}{h}(ik)\right)\right).$$

$$c_{33}=-(N_{x\tilde{t}}+\eta\Omega_x^2)\tau\beta^4(H^s_{xx}\beta^2+A_s).$$

$$c_{34}=\tau e_{31}\left(\beta^2\, cos(\beta z)\frac{dz}{dt}\phi-\left(\frac{2V_0e^{ik\tilde{t}}}{h}(ik)\right)\right).$$

$$m_{11}=-(1+\mu(z)^2\beta^2)I_0^*.$$

$$m_{12}=i(N_{x\tilde{t}}+\eta\Omega_x^2)\beta^2(1+\mu(z)^2\beta^2)I_1^*. \tag{45}$$

$$m_{13}=i(N_{x\tilde{t}}+\eta\Omega_x^2)\beta^2(1+\mu(z)^2\beta^2)J_1^*.$$

$$m_{22}=-(1+\mu(z)^2\beta^2)(I_0^*+I_2^*(N_{x\tilde{t}}+\eta\Omega_x^2)\beta^4).$$

$$m_{23}=-(1+\mu(z)^2\beta^2)(I_0^*+J_2^*(N_{x\tilde{t}}+\eta\Omega_x^2)\beta^4).$$

$$m_{33}=-(1+\mu(z)^2\beta^2)(I_0^*+K_2^*(N_{x\tilde{t}}+\eta\Omega_x^2)\beta^2).$$

$$m_{34}=(1+\mu(z)^2\beta^2)e_{31}\left(\beta^2\, cos(\beta z)\frac{dz}{d\tilde{t}}\phi-\left(\frac{2V_0e^{ik\tilde{t}}}{h}(ik)\right)\right).$$

4. Results and discussion

The behavior of an FG nanobeam submerged in a fluid, considering a variable nonlocal parameter, enhances the accuracy of the model, providing invaluable insights into structural deformation essential for optimizing performance across various engineering fields, including aerospace, biomechanics, and material science. This segment illustrates the responses of FG nanobeam submerged in a fluid medium on behalf of variable nonlocality.

The phase coefficients for the constituent materials $BaTiO_3$ and $CoFe_2O_4$ as discussed by the author (Ebrahimi *et al*. 2021) are specified in Table 1 and Table 2 comes with the property of Piezo electric PZT-4 (Ke *et al*. 2012). Furthermore, Table 3 demonstrates the relationship between electric voltage and magnetic potential by altering and raising nonlocal parameters. Notably, an elevated powerlaw index correlates with reduced $\Omega_x$and V_0. Table 4 validated the comparison between existing and present results of the natural frequency of submerged beams in water.

4.1 Effect of temperature gradient and nondimensional frequency over imperfection ratio

Variations in length due to thermal expansion can impact the imperfection ratio, as temperature changes lead to thermal stresses, altering stress and strain distribution within the nanobeam. Nondimensional frequency is also influenced by nonlocal parameters, whereas changes in nonlocal parameters can alter the mode and natural frequency. This redistribution interacts with existing imperfections, potentially altering the imperfection ratio.

Table 1 Material properties of $BaTiO_3$ and $CoFe_2O_4$

Material	Properties			
$BaTiO_3$	E[Pa]	166	e_{33} (N/m^{2}K)	(7.124x10^{-9})
	ρ [kg/m^3]	5800		
	ν [-]	1.1945	e_{15} (c/m^2)	14.1
$CoFe_2O_4$	E[Pa]	286	e_{31} (c/m^2)	-(4.1)
	ρ [kg/m^3]	5300		
	ν [-]	1.167	e_{11}(c/Vm)	(5.841x10^{-9})

Table 2 Material property of PZT – 4 (Ke *et al*. 2012)

	e_{31} (c/m^2)	e_{11}(c/Vm)	e_{33} (N/m^{2}K)	e_{15} (c/m^2)
PZT – 4	-4.1	5.841x10^{-9}	7.124x10^{-9}	14.1

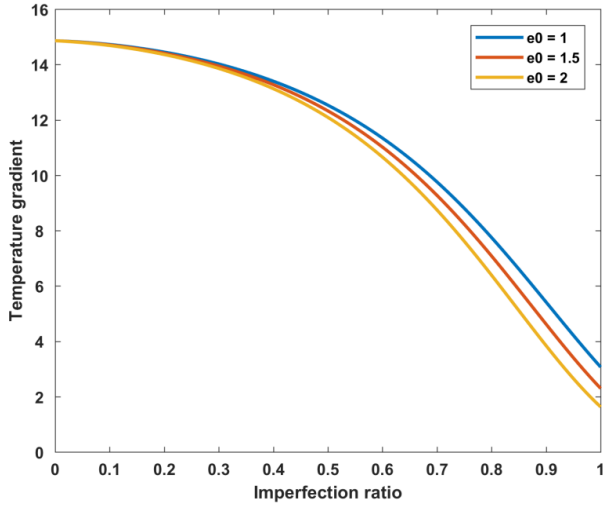

Fig. 2 Effect of nonlocality on temperature gradient and imperfection ratio

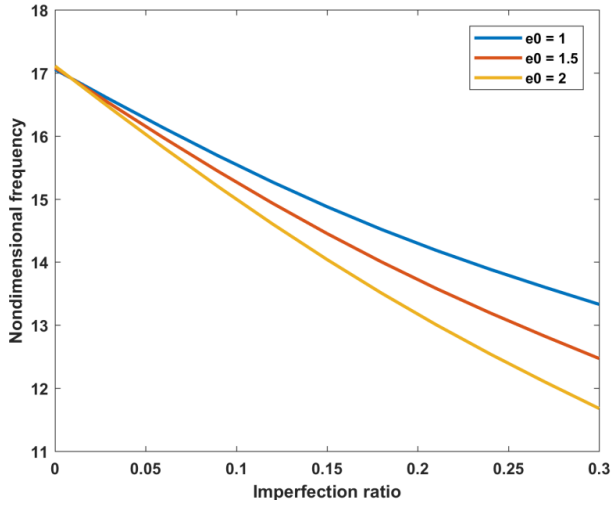

Fig. 3 Effect of nonlocality on dimensionless frequency and imperfection ratio

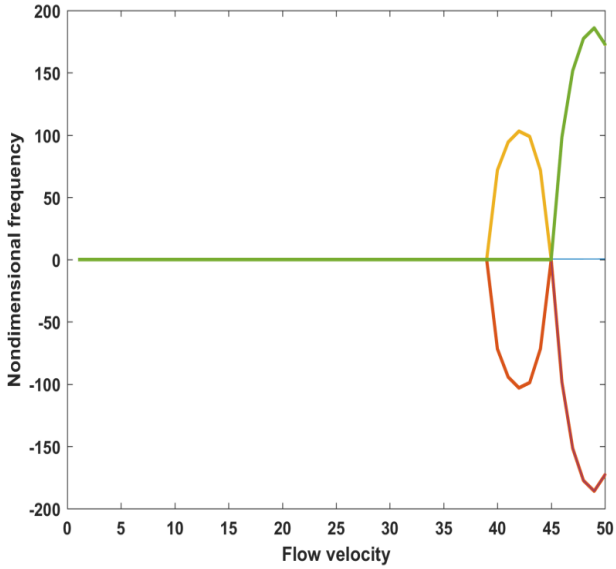

Fig. 4 Effect of nondimensional frequency overflow velocity in the context of ceramic nonlocal variable

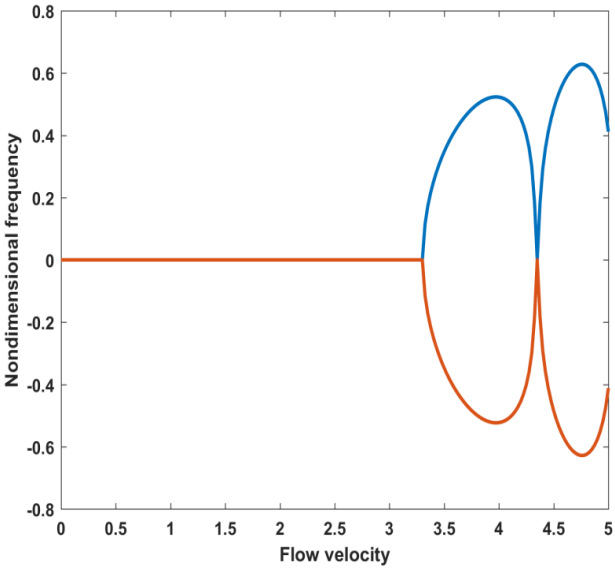

Fig. 5 Effect of nondimensional frequency overflow velocity in the context of metal nonlocal variable

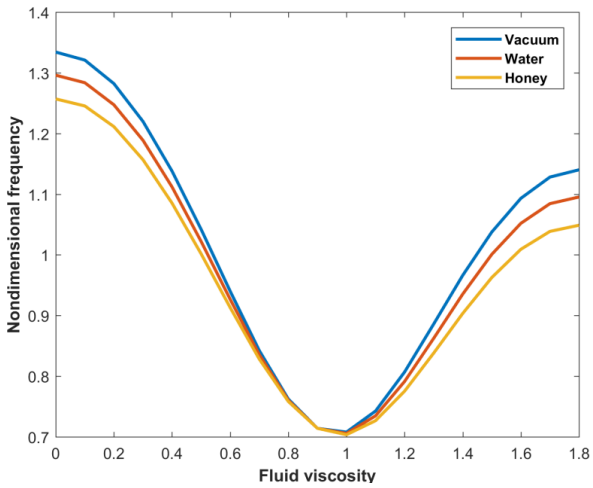

Fig. 6 Effect of nondimensional frequency on fluid viscosity with variants of viscous fluids for nonlocal metal variable

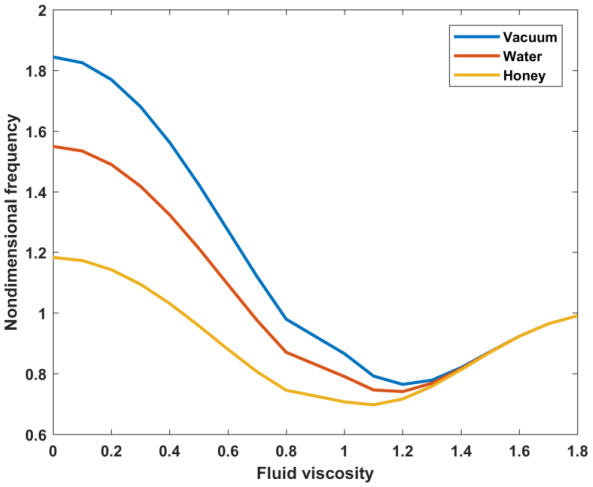

Fig. 7 Effect of nondimensional frequency on fluid viscosity with variants of viscous fluids for ceramic nonlocal variables

Table 3 Effect of powerlaw index, electric voltage, and magnetic potential with the natural frequency

Ω		$\tilde{p}$ = 0.2			$\tilde{p}$= 1			$\tilde{p}$= 5		
		V_0=-5	V_0=0	V_0=+5	V_0=-5	V_0=0	V_0=+5	V_0=-5	V_0=0	V_0=+5
0	Ω_x = -0.05	8.34927	7.68726	7.24086	8.36370	7.69636	7.24398	8.37810	7.70545	7.24711
	Ω_x = 0.00	8.34708	7.68034	7.22898	8.36151	7.68946	7.23212	8.37592	7.69856	7.23525
	Ω_x = -0.05	8.34489	7.67343	7.21709	8.35933	7.68255	7.22023	8.37373	7.69166	7.22337
1	Ω_x = -0.05	7.96429	7.33365	6.90880	7.97941	7.34319	6.91208	7.99450	7.35273	6.91536
	Ω_x = 0.00	7.96199	7.32641	6.89636	7.97712	7.33596	6.89964	7.99222	7.34550	6.90293
	Ω_x = 0.05	7.95969	7.31915	6.88389	7.97483	7.32872	6.88718	7.98993	7.33827	6.89047
2	Ω_x = -0.05	7.62789	7.02471	6.61874	7.64368	7.03468	6.62216	7.65944	7.04462	6.62558
	Ω_x = 0.00	7.62550	7.01715	6.60575	7.64129	7.02712	6.60917	7.65705	7.03708	6.61260
	Ω_x = 0.05	7.62310	7.00958	6.59273	7.63890	7.01956	6.59617	7.65466	7.02953	6.59960
3	Ω_x = -0.05	7.33065	6.75176	6.36250	7.34708	6.76213	6.36606	7.36347	6.77248	6.36962
	Ω_x = 0.00	7.32816	6.74389	6.34898	7.34459	6.75427	6.35255	7.36099	6.76463	6.35612
	Ω_x = 0.05	7.32566	6.73601	6.33544	7.34210	6.74640	6.33902	7.35850	6.75678	6.34259
		$\tilde{p}$= 7			$\tilde{p}$= 8			$\tilde{p}$= 10		
0	Ω_x = -0.05	8.55703	8.31260	8.37748	9.43205	8.84645	8.55259	10.2325	9.34987	8.72418
	Ω_x = 0.00	8.41640	7.88376	7.67745	9.30465	8.44476	7.86815	10.1152	8.97075	8.05433
	Ω_x = 0.05	8.27337	7.43021	6.90683	9.17548	8.02299	7.11820	9.99651	8.57489	7.32348
1	Ω_x = -0.05	8.08984	7.91790	8.03872	9.01035	8.47664	8.22104	9.84516	9.00077	8.39941
	Ω_x = 0.00	7.94094	7.46642	7.30630	8.87690	8.05654	7.50644	9.72317	8.60629	7.70137
	Ω_x = 0.05	7.78919	6.98583	6.49177	8.74141	7.61329	6.71622	9.59964	8.19284	6.93341
2	Ω_x = -0.05	7.67792	7.57252	7.74446	8.64241	8.15496	7.93354	9.50958	8.69849	8.11823
	Ω_x = 0.00	7.52087	7.09911	6.98123	8.50319	7.71737	7.19042	9.38323	8.28964	7.39369
	Ω_x = 0.05	7.36046	6.59180	6.12362	8.36165	7.25342	6.36107	9.25516	7.85955	6.58997
3	Ω_x = -0.05	7.31058	7.26690	7.48595	8.31777	7.87198	7.68141	9.21554	8.43377	7.87201
	Ω_x = 0.00	7.14545	6.77216	6.69332	8.17302	7.41771	6.91123	9.08510	8.01142	7.12247
	Ω_x = 0.05	6.97642	6.23831	5.79324	8.02566	6.93375	6.04369	8.95277	7.56553	6.28416

Fig. 2 presents the influence of varying nonlocal values (NLV) on the imperfection ratio (IR) at elevated temperatures. As the nonlocal value increases from 1.0 to 2.0, there is a notable trend of decreasing imperfection ratios. Specifically, when the nonlocal value is 1.0, the imperfection ratio decreases gradually. Additionally, with an increase in the nonlocal value to $e_0 = 1.5{,}2$ there is a further reductions in the imperfection ratio, respectively. In Fig. 3, at a nondimensional frequency of 17.0, the imperfection ratio decreases as the nonlocal increases with varying nonlocal values ($e_0 = 1{,}1.5{,}2$).

Higher nondimensional frequencies may influence the system's ability to resist imperfection growth, while increased nonlocal effects contribute to stabilizing the structure.

4.2 Effect of Nondimensional frequency on flow velocity and fluid viscosity

Fig. 4 shows the variation of nondimensional frequency overflow velocity within the context of the ceramic nonlocal variable. Increasing the nondimensional frequency with ceramic nonlocal variable influences the shifting points of the maximum flow velocity. Hence, with inital frequency levels, the flow velocity converges until a certain point and subsequently initiates resonance after the flow velocity reaches 35.0. Moreover, an elevated non-dimensional frequency of 50.0 results in heightened damping effects in the ceramic material, gradually reducing flow velocity within specific frequency ranges. Likewise, in Fig. 5, convergence occurred until a specific point, beyond which resonance phenomena were initiated. When the nondimensional frequency converges till the flow velocity reaches 3.0, the resonance behavior hits with the higher flow velocity. Also, there happens a damping when the flow velocity touches 4.4, along with increasing nondimensional frequencies in the context of metallic nonlocal variables.

4.3 Effect of Nondimensional frequency on fluid viscosity

At elevated nondimensional frequencies, viscosity becomes notably more influential, leading to a damping effect in honey. In Fig. 6, a gradual decrease in honey's behavior is observed, starting around 1.2 and damping at 1.0, exhibiting a resonant response driven by the influence

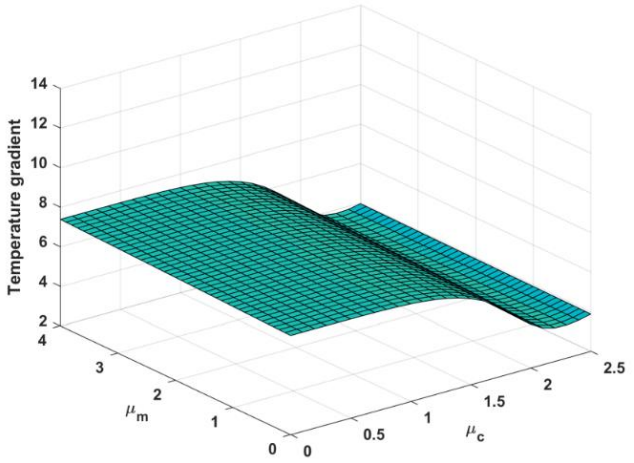

Fig. 8 Effect of variable nonlocal parameter with ceramic and metal phase (without fluid)

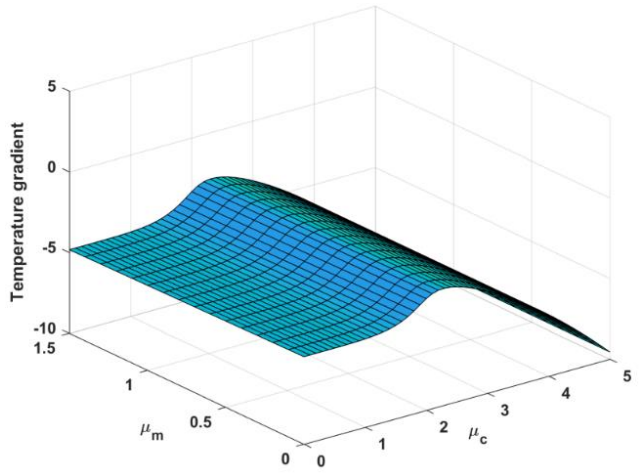

Fig. 9 Effect of variable nonlocal parameter with ceramic and metal phase (with fluid)

of the nonlocal metal variable at smaller scales. Conversely, with its inherently lower viscosity, water demonstrates less damping and a milder response to the nonlocal metal variable at smaller scales than honey. Furthermore, when contrasted with honey and water, vacuum responds more favorably to the dynamic interaction of nondimensional frequency and fluid viscosity. Similarly, in Fig. 7, the variation of nondimensional frequency over fluid viscosity in ceramic nonlocal variables has been studied. Comparing honey and water, honey shows a damping behavior, potentially influenced by ceramic nonlocal variables. Meanwhile, water shows moderate damping behavior. Hence, honey, water, and vacuum converge at some point.

4.4 Effect of variable nonlocal parameters (μ_c, μ_m) over temperature and magnetic field

The 3D curves in Figs. 8-11, represent the effect of ceramic and metal values on temperature and magnetic effect with and without fluid an environment. These figures manifest the dependence of the temperature and magnetic effect on the ceramic and metal base values. The fluid's coupling effect explains the damping nature of the physical parameters.

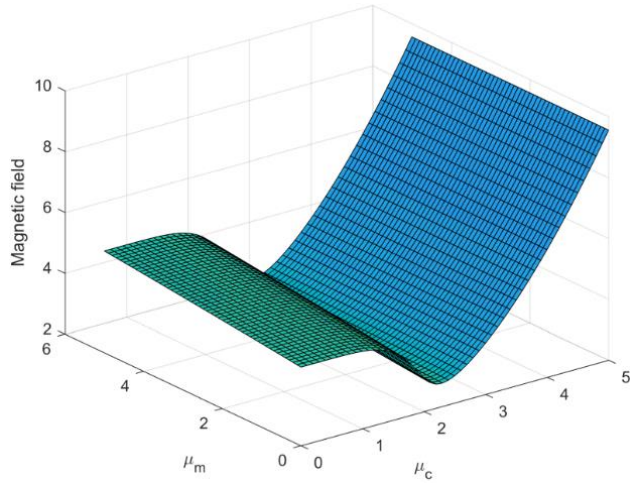

Fig. 10 Effect of magnetic field with ceramic and metal phase (without fluid)

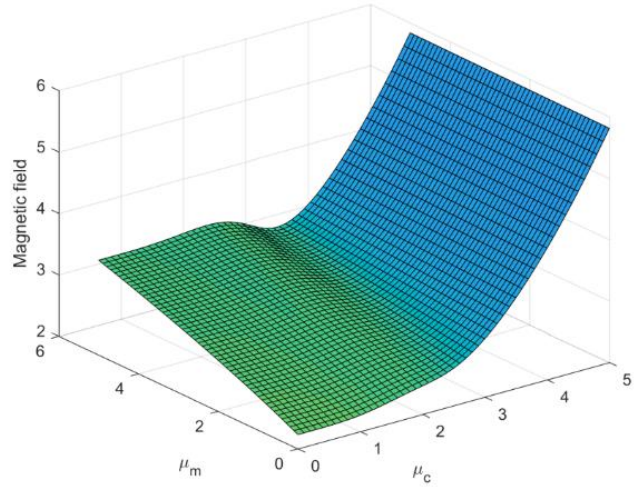

Fig. 11 Effect of magnetic field with ceramic and metal phase (with fluid)

Table 4 Validation of natural frequency of submerged beam in water

Mode No	Current study	Sheykhi *et al*. (2023)
Mode 1	294.537	295.437
Mode 2	907.354	907.464
Mode 3	1573.460	1573.460

5. Conclusions

The preceding study addresses the vibration analysis of a piezoelectric FG nanobeam submerged within the fluid. Hamilton's principle was employed to acquire the motion equations of the piezoelectric nanobeam. The derivation of the governing equations was acquired by adding the displacement field equations of the structure into the Euler-

Lagrange equations of the beam. These equations were then formulated as symmetric matrices using Navier's Solution method to obtain the necessary solutions. The significant outcomes of this research are highlighted as follows:

• The variable nonlocal parameter influences the interaction between the FG nanobeam and the surrounding fluid and affects the nanobeam's stiffness and dynamic response.

• The varying nonlocal parameter affects the stiffness of the ceramic phase and the mechanical properties of the metallic phase. Eventually, both phases experience a change in deformation.

• The influence of the variable nonlocal effect is contingent not only on the nanobeam's dimension and the variation of material components across its thickness.

• Raising the nondimensional frequency affects the shifting points of maximum flow velocity.

• At elevated nondimensional frequency, viscosity becomes more influential.

• In honey and water, both viscous fluids, significant fluid-structure interaction occurs, resulting in high damping effects. Mode shapes remain in vacuum but are altered in honey and water due to fluid-structure interaction.

The study's findings have some important areas to improve and can serve as benchmark results for future research. Our study may be limited by simplifications in the model, such as assumptions about material behavior or boundary conditions, which could affect the accuracy and applicability of our findings. Additionally, the scope of our study may not encompass all possible factors influencing the phenomenon under investigation. Future research could address these limitations by refining the model with more realistic assumptions, incorporating additional variables or complexities, and validating the findings through computational studies.

References

Adıyaman, G., Öner, E., Yaylacı, M. and Birinci, A. (2024), "The contact problem of a functionally graded layer under the effect of gravity", *ZAMM*, **103**(11), e202200560. https://doi.org/10.1002/zamm.202200560.

Alibeigi, B., Tadi Beni, Y. and Mehralian, F. (2018), "On the thermal buckling of magneto-electro-elastic piezoelectric nanobeams", *Eur. Phys. J. Plus.*, **133**, 133 https://doi.org/10.1140/epjp/i2018-11954-7.

Amara, K., Bouazza, M. and Fouad, B. (2016), "Postbuckling analysis of functionally graded beams using nonlinear model", *Period. Polytech. Mech. Eng.*, **60**(2), 121-128. https://doi.org/10.3311/PPme.8854.

Arpanahi, R.A. Eskandari, A., Mohammadi, B. and Hashemi, S.H. (2023a), "Study on the effect of viscosity and fluid flow on buckling behavior of nanoplate with surface energy", *Results Eng.*, **18**, 101078. https://doi.org/10.1016/j.rineng.2023.101078.

Arpanahi, R.A., Mohammadi, B., Ahmadian, M.T. and Hashemi, S.H. (2023b), "Study on the buckling behavior of nonlocal nanoplate submerged in viscous moving fluid", *Int. J. Dyn. Control*, **11**, 2820-2830. https://doi.org/10.1007/s40435-023-01166-w.

Barretta, R., Fabbrocino, F., Luciano, R. and de Sciarra, F.M. (2018), "Closed-form solutions in stress-driven two-phase integral elasticity for bending of functionally graded nano-beams", *Phys. E*, **97**, 13-30. https://doi.org/10.1016/j.physe.2017.09.026.

Becheri, T., Amara, K., Bouazza, M. and Benseddiq, N. (2016), Buckling of symmetrically laminated plates using nth-order shear deformation theory with curvature effects", *Steel Compos. Struct.*, **21**(6), 1347-1368. https://doi.org/10.12989/scs.2016.21.6.1347.

Boucheta, A., Bouazza, M., Becheri, T., Eltaher, M.A, Tounsi, A. and Benseddiq, N. (2024), "Bending of sandwich FGM plates with a homogeneous core either hard or soft via a refined hyperbolic shear deformation plate theory", *Iran J. Sci. Technol. Trans. Civ. Eng.*, 1-15. https://doi.org/10.1007/s40996-024-01386-w.

Bouazza, M., Becheri, T., Boucheta, A., Eltaher, M.A. and Benseddiq, N. (2019a), "Bending behavior of laminated composite plates using the refined four-variable theory and the finite element method", *Earthq. Struct.*, **17**(3), 257-270. https://doi.org/10.12989/eas.2019.17.3.257.

Bouazza, M., Antar, K., Amara, K., Benyoucef, S. and Bedia, E.A.A. (2019b), "Influence of temperature on the beams behavior strengthened by bonded composite plates", *Geomech. Eng.*,**18**(5), 555-66. https://doi.org/10.12989/gae.2019.18.5.555.

Cuong-Le, T., Nguyen, K.D., Le-Minh, H., Phan-Vu, P., Nguyen-Trong, P. and Tounsi, A. (2022), "Nonlinear bending analysis of porous sigmoid FGM nanoplate via IGA and nonlocal strain gradient theory", *Adv. Nano Res.*, **12**(5), 441-455. https://doi.org/10.12989/anr.2022.12.5.441.

Dehshahri, K., Nejad, M.Z., Ziaee, S., Niknejad, A. and Hadi, A. (2020), "Free vibrations analysis of arbitrary three-dimensionally FGM nanoplates", *Adv. Nano Res.*, **8**(2), 115-134. https://doi.org/10.12989/anr.2020.8.2.115.

Derbale, A., Bouazza, M. and Benseddiq, N. (2021), "Analysis of the mechanical and thermal buckling of laminated beams by new refined shear deformation theory", *Iran J. Sci. Technol. Trans. Civ. Eng.*, **45**, 89-98. https://doi.org/10.1007/s40996-020-00417-6.

Ebrahimi, F., Karimiasl, M. and Selvamani, R. (2020), "Bending analysis of magneto-electro piezoelectric nanobeams system under hygro-thermal loading", *Adv. Nano Res.*, **8**(3), 203-214. https://doi.org/10.12989/anr.2020.8.3.203.

Ebrahimi, F., Khosravi, K. and Dabbagh, A. (2021), "Wave dispersion in viscoelastic FG nanobeam via a novel spatial - temporal nonlocal strain gradient framework", *Wave Random Complex Med.*, 1-23. https://doi.org/10.1080/17455030.2021.1970282.

Ellali, M., Amara, K., Bouazza, M. and Bourada, F. (2018), "The buckling of piezoelectric plates on pasternak elastic foundation using higher-order shear deformation plate theories", *Smart Struct. Syst.*, **21**(1), 113-122. https://doi.org/10.12989/sss.2018.21.1.113.

Ellali, M., Bouazza, M. and Amara, K. (2019), "Thermal buckling of a sandwich beam attached with piezoelectric layers via the shear deformation theory", *Arch. Appl. Mech.*, **92**, 657-665. https://doi.org/10.1007/s00419-021-02094-x.

Ellali, M., Bouazza, M. and Zenkour, A.M. (2022), "Impact of micromechanical approaches on wave propagation of FG plates via indeterminate integral variables with a hyperbolic secant shear model", *Int. J. Comput. Methods.*, **19**(9). https://doi.org/10.1142/S0219876222500190.

Ellali, M., Bouazza, M. and Zenkour, A.M. (2023a), "Wave propagation in functionally-graded nanoplates embedded in a winkler-pasternak foundation with initial stress effect", *Phys. Mesomech.*, **26**, 282-294. https://doi.org/10.1134/S1029959923030049.

Ellali, M., Bouazza, M. and Zenkour, A.M. (2023b), "Wave propagation of FGM plate via new integral inverse cotangential shear model with temperature-dependent material properties",

Geomech. Eng., **33**(5), 427-437. https://doi.org/10.12989/gae.2023.33.5.427.

Ellali, M., Amara, K. and Bouazza, M. (2024), "Thermal buckling of porous FGM plate integrated surface-bonded piezoelectric", *CSM.*, **13**(2), 171-186. https://doi.org/10.12989/csm.2024.13.2.171.

Ghamkhar, M., Harbaoui, I., Hussain, M., Ayed, H., Khadimallah, M.A. and Alshoaibi, A. (2022), "Structural monitoring of layered FGM distribution ring support: Analysis with and without internal pressure", *Adv. Nano Res.*, **12**(3), 337-344. https://doi.org/10.12989/anr.2022.12.3.337.

Heidari, F., Afsari, A. and Janghorban, M. (2020), "Several models for bending and buckling behaviors of FG-CNTRCs with piezoelectric layers including size effects", *Adv. Nano Res.*, **9**(3), 193-210. https://doi.org/10.12989/anr.2020.9.3.193.

Kaur, I. and Singh, K. (2022), "Functionally graded nonlocal thermoelastic nanobeam with memory-dependent derivatives", *SN Appl. Sci.*, **4**, 329. https://doi.org/10.1007/s42452-022-05212-8.

Kaur, I. and Singh, K. (2023a), "Forced flexural vibrations due to time-harmonic source in a thin nonlocal rectangular plate with memory-dependent derivative", *Mech. Solids*, **58**, 1257-1270. https://doi.org/10.3103/S0025654423600538.

Kaur, I. and Singh, K. (2023b), "Nonlocal memory dependent derivative analysis of a photo-thermoelastic semiconductor resonator", *Mech. Solids*, **58**, 529-553. https://doi.org/10.3103/S0025654422601094.

Kaur, I., Lata, P. and Singh, K. (2022), "Thermoelastic damping in generalized simply supported piezo-thermo-elastic nanobeam", *Struct. Eng. Mech.*, **81**(1), 29-37. https://doi.org/10.12989/sem.2022.81.1.029.

Kaur, I., Singh, K. and Ghita, G.M.D. (2021), "New analytical method for dynamic response of thermoelastic damping in simply supported generalized piezothermoelastic nanobeam", *Z. Angew. Math. Mech.*, **101**, e202100108. https://doi.org/10.1002/zamm.202100108.

Ke, L.L. and Wang, Y.S. (2014), "Free vibration of size-dependent magneto-electro-elastic nanobeams based on the nonlocal theory", *Phys. E*, **63**, 52-61. https://doi.org/10.1016/j.physe.2014.05.002.

Ke, L.L., Wang, Y.S. and Wang, Z.D. (2012), "Nonlinear vibration of piezoelectric based on the nonlocal theory", *Compos. Struct.*, **94**, 2038-2047. https://doi.org/10.1016/j.compstruct.2012.01.023.

Kiani, Y., Eslami, M.R. (2010), "Thermal buckling analysis of functionally graded material beams", *Int. J. Mech. Mater. Des.*, **6**, 229-238. https://doi.org/10.1007/s10999-010-9132-4.

Lafi, D.E., Bouhadra, A., Mamen, B., Menasria, A., *et al.* (2024), "Combined influence of variable distribution models and boundary conditions on the thermodynamic behavior of FG sandwich plates lying on various elastic foundations", *Struct. Eng. Mech.*, **89**(2), 103-119. https://doi.org/10.12989/sem.2024.89.2.103.

Li, H.C., Ke, L.L, Yang, J., Kitipornchai, S. and Wang, Y.S. (2020), "Free vibration of variable thickness FGM beam submerged in fluid", *Compos. Struct.*, **233**, 111582. https://doi.org/10.1016/j.compstruct.2019.111582.

Li, L. and Hu, Y. (2016), "Nonlinear and free vibration analysis of nonlocal strain gradient beams made of functionally graded material", *Int. J. Eng. Sci.*, **102**, 77-92. https://doi.org/10.1016/j.ijengsci.2016.07.011.

Li, S.R., Su, H.D. and Cheng, C.J. (2009), "Free vibration of functionally graded material beams with surface-bonded piezoelectric layers in thermal environment", *Appl. Math. Mech.*, **30**, 969-82. https://doi.org/10.1007/s10483-009-0803-7.

Lim, C.W., Zhang, G. and Reddy, J.N. (2015), "A higher-order nonlocal elasticity and strain gradient theory and its applications in wave propagation", *J. Mech. Phys. Solids*, **78**, 298-313. https://doi.org/10.1016/j.jmps.2015.02.001.

Nguyen, T.K., Nguyen, T.T.P., Vo, T.P. and Thai, H.T. (2015), "Vibration and buckling analysis of functionally graded sandwich beams by a new higher-order shear deformation theory", *Compos. B. Eng.*, **76**, 273-285. https://doi.org/10.1016/j.compositesb.2015.02.032.

Parsa, A. and Mahmoudpour, E. (2019), "Nonlinear free vibration analysis of embedded flexoelectric curved nanobeams conveying fluid and submerged in fluid via nonlocal strain gradient elasticity theory", *Microsyst. Technol.*, **25**, 4323-4339. https://doi.org/10.1007/s00542-019-04408-0.

Reddy, J.N. and El-Borgi, S. (2014), "Eringen's nonlocal theories of beams accounting for moderate rotations", *Int. J. Eng. Sci.*, **82**, 159-177. https://doi.org/10.1016/j.ijengsci.2014.05.006.

Romano, G. and Barretta, R. (2017), "Stress-driven versus strain-driven nonlocal integral model for elastic nano-beams", *Compos. B. Eng.*, **114**, 184-188. https://doi.org/10.1016/j.compositesb.2017.01.008.

Shariati, A, Ebrahimi, F., Karimiasl, M., Vinyas, M. and Toghroli, A. (2020b), "On transient hygrothermal vibration of embedded viscoelastic flexoelectric/piezoelectric nanobeams under magnetic loading", *Adv. Nano Res.*, **8**(1), 49-58. https://doi.org/10.12989/anr.2020.8.1.049.

Shariati, A., Ebrahimi, F., Karimiasl, M., Selvamani, R. and Toghroli, A. (2020a), "On bending characteristics of smart magneto-electro-piezoelectric nanobeams system", *Adv. Nano Res.*, **9**(3), 183-191. https://doi.org/10.12989/anr.2020.9.3.183.

Sheykhi, M., Eskandari, A., Ghafari, D., Arpanahi, R.A., Mohammadi, B. and Sh. Hashemi, H. (2023), "Investigation of fluid viscosity and density on vibration of nano beam submerged in fluid considering nonlocal elasticity theory", *Alex. Eng. J.*, **65**, 607-614. https://doi.org/10.1016/j.aej.2022.10.016.

Sun, D. and Luo, S.N. (2011), "Wave propagation of functionally graded material plates in thermal environments", *Ultrasonics*, **51**(8), 940-952. https://doi.org/10.1016/j.ultras.2011.05.009.

Thai, H.T. and Choi, D. H. (2012), "A refined shear deformation theory for free vibration of functionally graded plates on elastic foundation", *Compos. B. Eng.*, **43**(5), 2335-2347. https://doi.org/10.1016/j.compositesb.2011.11.062.

Thai, H.T., Park, T. and Choi, D.H. (2012), "An efficient shear deformation theory for vibration of functionally graded plates", *Arch. Appl. Mech.*, **83**, 137-149. https://doi.org/10.1007/s00419-012-0642-4.

Turan, M., Uzun Yaylacı, E. and Yaylacı, M. (2023), "Free vibration and buckling of functionally graded porous beams using analytical, finite element, and artificial neural network methods", *Arch. Appl. Mech.*, **93**, 1351-1372. https://doi.org/10.1007/s00419-022-02332-w.

Vinh, P.V. and Tounsi, A. (2022a), "Free vibration analysis of functionally graded doubly curved nanoshells using nonlocal first-order shear deformation theory with variable nonlocal parameters", *Thin Wall. Struct.*, **174**, 109084. https://doi.org/10.1016/j.tws.2022.109084.

Vinh, P.V. and Tounsi, A. (2022b), "The role of spatial vibration of the nonlocal parameter on the free vibration of functionally graded sandwich nanoplates", *Eng. Comput.*, **38**(5), 4301-4319. https://doi.org/10.1007/s00366-021-01475-8.

Vinh, P.V., Tounsi, A. and Belarbi, M.O. (2023), "On the nonlocal free vibration analysis of functionally graded porous doubly curved shallow nanoshells with variable nonlocal parameters", *Eng. Comput.*, **39**, 835-855. https://doi.org/10.1007/s00366-022-01687-6.

Yaylacı, M., Abanoz, M., Uzun Yaylacı, E., Ölmez, H., Sekban, M.D. and Birinci, A. (2022), "The contact problem of the functionally graded layer resting on rigid foundation pressed via rigid punch", *Steel Compos. Struct.*, **43**(5), 661-672.

https://doi.org/10.12989/scs.2022.43.5.661.
Yaylacı, M., Öner, E., Adıyaman, G., Öztürk, Ş., Uzun Yaylacı, E. and Birinci, A. (2023), "Analyzing of continuous and discontinuous contact problems of a functionally graded layer: theory of elasticity and finite element method", *Mech. Based Des. Struct.*, 1-19. https://doi.org/10.1080/15397734.2023.2262562.
Yaylacı, M., Uzun Yaylacı, E., Turan, M., Özdemir, M.E., Öztürk, Ş. and Ay, S. (2024), "Research of the crack problem of a functionally graded layer", *Steel Compos. Struct.*, **50**(1), 77-87. https://doi.org/10.12989/scs.2024.50.1.077.

CC